catalysts

MDPI

Article

Effect of Brønsted Acid on the Reactivity and Selectivity of the Oxoiron(V) Intermediates in C-H and C=C Oxidation Reactions

Alexandra M. Zima, Oleg Y. Lyakin, Anna A. Bryliakova, Dmitrii E. Babushkin, Konstantin P. Bryliakov and Evgenii P. Talsi *

Boreskov Institute of Catalysis, Pr. Lavrentieva 5, 630090 Novosibirsk, Russia
* Correspondence: talsi@catalysis.ru

Abstract: The effect of $HClO_4$ on the reactivity and selectivity of the catalyst systems **1**,**2**/H_2O_2/AcOH, based on nonheme iron complexes of the PDP families, [(^{Me2OMe}PDP)Fe^{III}(μ-OH)$_2$Fe^{III}(^{MeOMe2}PDP)](OTf)$_4$ (**1**) and [(^{NMe2}PDP)Fe^{III}(μ-OH)$_2$Fe^{III}(^{NMe2}PDP](OTf)$_4$ (**2**), toward oxidation of benzylideneacetone (**bna**), adamantane (**ada**), and (3a*R*)-(+)-sclareolide (**S**) has been studied. Adding $HClO_4$ (2–10 equiv. vs. Fe) has been found to result in the simultaneous improvement of the observed catalytic efficiency (i.e., product yields) and the oxidation regio- or enantioselectivity. At the same time, $HClO_4$ causes a threefold increase of the second-order rate constant for the reaction of the key oxygen-transferring intermediate [(^{Me2OMe}PDP)Fe^{V}=O(OAc)]$^{2+}$ (**1a**), with cyclohexane at −70 °C. The effect of strong Brønsted acid on the catalytic reactivity is discussed in terms of the reversible protonation of the Fe=O moiety of the parent perferryl intermediates.

Keywords: C-H activation; oxidation; iron; intermediate; mechanism; non-heme

check for updates

Citation: Zima, A.M.; Lyakin, O.Y.; Bryliakova, A.A.; Babushkin, D.E.; Bryliakov, K.P.; Talsi, E.P. Effect of Brønsted Acid on the Reactivity and Selectivity of the Oxoiron(V) Intermediates in C-H and C=C Oxidation Reactions. *Catalysts* **2022**, *12*, 949. https://doi.org/10.3390/catal12090949

Academic Editor: Maria Jaworska

Received: 9 August 2022
Accepted: 22 August 2022
Published: 26 August 2022

1. Introduction

High-valent iron-oxo complexes are generally accepted to be the key intermediates of metalloenzyme-mediated oxidations in living nature, as well as in some bioinspired model catalyst systems based on iron complexes and hydrogen peroxide [1–22].

For nonheme, iron-containing enzymes, both iron(IV)- and iron(V)-oxo species have been proposed as active intermediates [11–23]. However, while the involvement of the iron(IV)-oxo intermediates in enzymatic oxidations is firmly established, there are still no experimental data witnessing the participation of the nonheme iron(V)-oxo intermediates in these oxidations [18,19].

In contrast to enzymatic systems, for model nonheme iron-based systems, there have been several examples of spectroscopically characterized iron(V)-oxo intermediates relevant to catalytic transformations (Figure 1) [24–33]. The comparison of the reactivities of nonheme Fe^{IV}=O and Fe^{V}=O species bearing the same macrocyclic ligand bTAML (Figure 1) has shown that even after correcting for the pH difference, the second-order rate constant for benzyl alcohol oxidation by Fe(V)=O at pH 7 is 2500 times higher than that for Fe(IV)=O at pH = 12 [34]. The reactivity studies of Fe^{V}=O and Fe^{IV}=O species supported by the same tetradentate N-donor PyNMe$_3$ ligand (Figure 1) have shown that Fe^{V}=O accomplishes hydrogen atom transfer (HAT) from C-H groups 4 to 5 orders of magnitude faster than Fe^{IV}=O [35].

It was established that Brønsted and Lewis acids are able to enhance the oxidizing power of nonheme Fe^{IV}=O complexes [36–44]. It was also shown that acids trigger O-O bond heterolysis of nonheme Fe^{III}(OOH) precursor species to facilitate the formation of the active intermediates capable of hydroxylating strong C-H bonds [45,46]. However, those intermediates (presumably Fe^{V}=O) have not been observed spectroscopically.

It was shown previously that the catalyst system **1**/H_2O_2/AcOH, where **1** is the [(^{Me2OMe}PDP)Fe^{III}(μ-OH)$_2$Fe^{III}(^{MeOMe2}PDP)](OTf)$_4$ complex (^{Me2OMe}PDP is 3,5-Me$_2$,4-OMe

substituted (*S*,*S*)-PDP ligand) and AA is acetic acid, exhibits the oxoiron(V) intermediate **1a** (g_1 = 2.07, g_2 = 2.01, g_3 = 1.96) [47]. This intermediate can be assigned to the low-spin $[(^{Me2OMe}PDP)Fe^{V}{=}O(OAc)]^{2+}$ species on the basis of the identity of its EPR spectrum to that of the $Fe^{V}{=}O$ intermediate observed in the catalyst system $[(MeO\text{-}PyNMe_3)Fe^{II}(CF_3SO_3)_2]$/CPCA (CPCA-cyclohexyl peroxycarboxylic acid) (Figure 1). The assignment of the Fe^{V} oxidation state of the latter intermediate was supported by Mössbauer spectroscopy [32]. In the figure above, **1a** directly oxidizes alkenes [47], alkanes [48] and arenes [49] at −70 °C.

The system **2**/H_2O_2/AA (**2** is $[(^{NMe2}PDP)Fe^{III}(\mu\text{-}OH)_2Fe^{III}(^{NMe2}PDP](OTf)_4$, complex (^{NMe2}PDP is 4-NMe_2 substituted (*S*,*S*)-PDP ligand) displays the EPR spectrum of the high-spin intermediate **2a** (g_1 = 4.30, g_2 = 3.69, g_3 = 1.96). In the figure above, **2a**, which reacts with cyclohexene and cyclohexane at −40 °C, has been assigned to the high-spin (*S* = 3/2) oxoiron(V) species $[(^{NMe2}PDP)Fe^{V}{=}O(OAc)]^{2+}$ (Figure 1) [50–52].

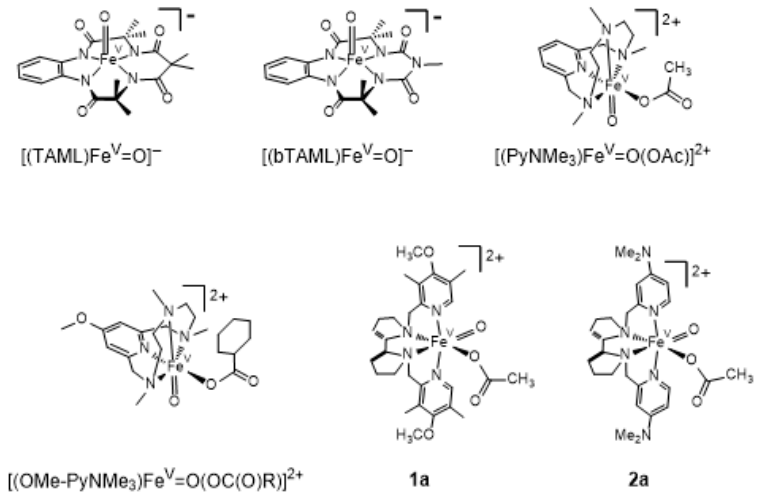

Figure 1. Spectroscopically characterized oxoiron(V) complexes [24,26,31,32,47,51].

In this work, we scrutinized the effect of Brønsted acid ($HClO_4$) on the oxidation of C=C and C-H groups of various organic substrates (Figure 2) by the catalyst systems **1**/H_2O_2/AA and **2**/H_2O_2/AA. The observed correlations between the stability and reactivity of **1a** and **2a** and the chemo-, regio-, and stereoselectivities of the corresponding catalyst systems are discussed.

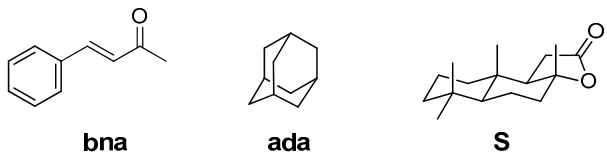

Figure 2. The structures of organic substrates studied.

2. Results

2.1. Effect of $HClO_4$ on the Catalyst Systems 1/H_2O_2/AA and 2/H_2O_2/AA: EPR Data

As was shown previously [47], the putative oxoiron(V) intermediate $[(^{Me2OMe}PDP)Fe^{V}{=}O(OAc)]^{2+}$ (**1a**) can be detected by EPR in the catalyst system **1**/H_2O_2/AA ([1] = 0.02 M) at low temperature (Figure 3a).

The intermediate **1a** is unstable and decays with the first-order rate constant $k_1 = (1.8 \pm 0.2) \times 10^{-3}$ s^{-1} at −70 °C. This decay of **1a** is accelerated by the addition of cyclohexane. The corresponding second-order rate constant k_2 for the reaction of **1a** with cyclohexane at −70 °C is $(2 \pm 0.4) \times 10^{-3}$ M^{-1} s^{-1} [48]. Adding 2 equiv. (vs. Fe) of $HClO_4$ to the catalyst system **1**/H_2O_2/AA at −70 °C reduces the stability of **1a**, resulting in a threefold increase of the rate constant of **1a** self-decay ($k_1 = (6 \pm 0.5) \times 10^{-3}$ s^{-1}). It is

worth noting that, while affecting the stability of **1a**, adding $HClO_4$ does not visibly change the parameters of its EPR spectrum, which is evidence that $HClO_4$ does not interfere with the first coordination sphere of the central atom. Adding 5 equiv. (vs. Fe) of $HClO_4$ to the catalyst system **1**/AcOOH/AA/C_6H_{12} (1:3:10:10) at −70 °C increases by factor of 2.5 the second-order rate constant k_2 of the reaction of **1a** with cyclohexane, demonstrating the positive effect of $HClO_4$ on the C-H oxidation reactivity of **1a**.

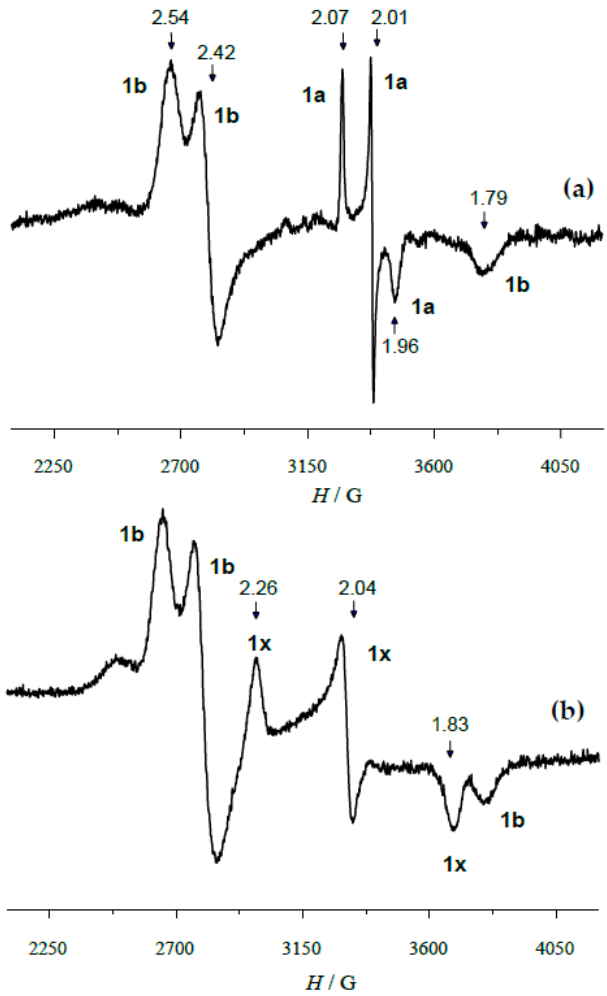

Figure 3. EPR spectrum (−196 °C) of the catalyst system **1**/H_2O_2/AA = 1:3:5 ([1] = 0.02 M) in a CH_2Cl_2/CH_3CN (1.8:1 *v*/*v*) mixture recorded 3 min after mixing the reagents at −75 °C (**a**). EPR spectrum (−196 °C) of the sample **1**/H_2O_2//$HClO_4$ = 1:3:2 ([1] = 0.02 M) in a CH_2Cl_2/CH_3CN (1.8:1 *v*/*v*) mixture recorded 6 min after mixing the reagents at −40 °C (**b**). The signals denoted by symbol **1b** belongs to the stable ferric complex $[(^{Me2OMe}PDP)Fe^{III}(OAc)]^{2+}$.

The catalyst system **1**/H_2O_2/$HClO_4$ = 1:3:2, containing no acetic acid, exhibits a novel intermediate **1x**. The EPR spectrum of **1x** (g_1 = 2.26, g_2 = 2.04, g_3 = 1.83, Figure 3b) markedly differs from that of **1a** (g_1 = 2.07, g_2 = 2.01, g_3 = 1.96, Figure 3a). The intermediate **1x** is more stable than **1a** and decays with the self-decay rate constant emphk = (1 ± 0.2) × 10^{-3} s^{-1} only at −40 °C, while **1a** decays with a comparable rate at −70 °C [48]. The EPR parameters of **1x** (g_1 = 2.26, g_2 = 2.04, g_3 = 1.83) are rather close to those of activated bleomycin (g_1 = 2.26, g_2 = 2.17, g_3 = 1.94) [49], which is a well-established ferric hydroperoxo complex. The intermediate **1x** could be assigned to a ferric hydroperoxo complex $[(^{Me2OMe}PDP)Fe^{III}(OOH)(CH_3CN)]^{2+}$; In the presence of acetic acid, **1x** would rapidly exchange its CH_3CN with AcO^- and further give **1a.** In agreement with its ferric hydroperoxo nature, **1x** is inert toward cyclohexane at −40 °C (whereas **1a** reacts with this

substrate even at −70 °C). These data suggest that additives of $HClO_4$ can affect the catalytic properties of the system **1**/H_2O_2/AA by enhancing the reactivity of the oxidizing intermediate [(^{Me2OMe}PDP)Fe^V=O(OAc)]$^{2+}$ (**1a**). The contribution of the intermediate [(^{Me2OMe}PDP)Fe^{III}(OOH)(CH_3CN)]$^{2+}$ (**1x**) to the catalytic reaction should not be significant, since **1x** cannot compete with **1a** in aliphatic C-H oxidations.

Attempts to detect reactive iron-oxygen intermediates in the catalyst system **2**/H_2O_2/$HClO_4$ using EPR spectroscopy were unsuccessful, whereas intermediate **2a** could be readily observed in the catalyst system **2**/H_2O_2/AA at −40 °C [53,54]. Previously, it was established that the active species of the catalyst system **2**/H_2O_2/AA = 1:3:10 was the high-spin (S = 3/2) iron-oxygen intermediate with a proposed structure [(^{NMe2}PDP)Fe^V=O(OAc)]$^{2+}$ (**2a**) (g_1 = 4.36, g_2 = 3.69, g_3 = 1.96) (Figure 4a) [50–54]. The intermediate **2a** decays with the rate constant $k = (2 \pm 0.2) \times 10^{-3}$ s^{-1} at −40 °C [52]. Like in the case of **1a**, the presence of $HClO_4$ does not alter the EPR spectrum of **2a** (Figure 4b). However, adding $HClO_4$ (2 equiv. vs. Fe) accelerates the self-decay of **2a** ($k = (5 \pm 0.5) \times 10^{-3}$ s^{-1} at −40 °C, ([$HClO_4$] = 0.08 M). The high-spin intermediate **2a** is less reactive toward C=C and C-H groups than the low-spin intermediate **1a**: while **1a** reacts with cyclohexene and cyclohexane at −70 °C [48], **2a** displays comparable reactivity toward these substrates only at −40 °C [52,53].

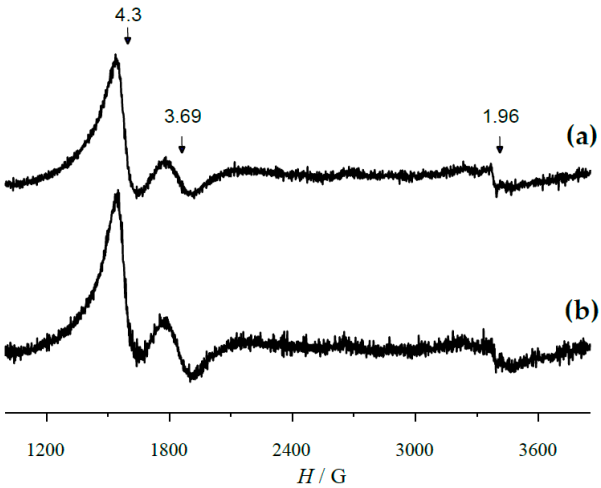

Figure 4. EPR spectrum (−196 °C) of the catalyst system **2**/H_2O_2/AA = 1:3:10 ([**2**] = 0.02 M) in a 1:1.8 CH_3CN/CH_2Cl_2 mixture, recorded 1.5 min after mixing the reagents at −75 °C (**a**). EPR spectrum (−196 °C) of the sample in "a," recorded 1.5 min after the addition of 2 equiv. of $HClO_4$ (**b**).

2.2. Enantioselective Oxidation of Benzylideneacetone by the Catalyst Systems 1/H_2O_2/AA and 2/H_2O_2/AA

The catalyst systems **1**/H_2O_2/$HClO_4$, **1**/H_2O_2/AA, and **1**/H_2O_2/AA/$HClO_4$ have been compared in the enantioselective oxidation of benzylideneacetone (**bna**) (Table 1). It can be seen that the enantioselectivities of these catalyst systems are rather close (34–36% *ee*, entries 1–3, Table 1). This result has been rather unexpected because different intermediates were detected in the catalyst systems **1**/H_2O_2/$HClO_4$ and **1**/H_2O_2/AA (**1x** and **1a**, respectively). Apparently, **1x** rapidly converts into the intermediate [(^{Me2OMe}PDP)Fe^V=O(S)]$^{2+}$ (**1a′**, where S = CH_3CN or H_2O) under the conditions of the catalytic experiment (0 °C). We believe that intermediates [(^{Me2OMe}PDP)Fe^V=O(OAc)]$^{2+}$ (**1a**) and **1a′** have close structures and therefore, should display close epoxide yields and enantioselectivities in **bna** oxidation (Table 1).

It is worth noting that the yield of the oxidation product is reasonably higher for the **1**/H_2O_2/AA/$HClO_4$ system than for the systems **1**/H_2O_2/$HClO_4$ and **1**/H_2O_2/AA (89% vs. 52–61%, entries 1 and 2 vs. entry 3, Table 1). The likely reason of this difference is the $HClO_4$-induced reactivity enhancement of the intermediate **1a**, operating in the system **1**/H_2O_2/AA/$HClO_4$.

Table 1. The effect of $HClO_4$ on the asymmetric epoxidation of benzylideneacetone with H_2O_2 in the presence of complexes **1** and **2** [a].

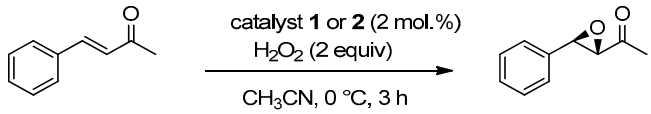

Entry	Catalyst	Carboxylic Acid	Strong Acid	Epoxide Yield (%)	*ee* (%)
1	**1**	—	$HClO_4$	52	34
2	**1**	AA	—	61	35
3	**1**	AA	$HClO_4$	89	36
4	**1**	EHA	—	44	63
5	**1**	EHA	$HClO_4$	13	66
6	**2**	—	$HClO_4$	12	46
7 [b]	**2**	AA	—	11	59
8	**2**	AA	$HClO_4$	5	51
9	**2**	EHA	—	58	85
10	**2**	EHA	$HClO_4$	2	— [c]

[a] At 0 °C, [catalyst]:[substrate]:[H_2O_2]:[acetic acid]:[$HClO_4$] = 1 μmol:100 μmol:200 μmol:55 μmol:10 μmol; oxidant was added by a syringe pump over 30 min, and the mixture was stirred for an additional 2.5 h, followed by NMR and HPLC analysis. [b] From ref. [54]. [c] Not measured.

Replacing acetic acid with 2-ethylhexanoic acid (EHA) leads to a larger difference between the enantioselectivities of the systems **1**/H_2O_2/$HClO_4$ and **1**/H_2O_2/EHA/($HClO_4$) (Table 1, entries 4 and 5 vs. 1), thus clearly witnessing that carboxylic acid is present in the structure of the active perferryl species at the step of enantioselective oxygen transfer in both systems (**1**/H_2O_2/EHA and **1**/H_2O_2/EHA/$HClO_4$). The unexpectedly low epoxide yield in the latter case (Table 1, entry 5) may reflect the possibility that the effect of $HClO_4$ on the intermediate $[(^{Me2OMe}PDP)Fe^{V}{=}O(OC(O)C_7H_{15})]^{2+}$ (**1a**$^{\mathbf{EHA}}$) [55] is more destabilizing than activating towards selective epoxidation, thus resulting in rapid catalyst degradation after only a few catalytic turnovers.

The epoxide yield in the catalyst system **2**/H_2O_2/AA/**bna** is much lower than that in the catalyst system **1**/H_2O_2/AA/**bna** (11% vs. 61%, entry 7, Table 1 vs. entry 2, Table 1), which most likely reflects a higher contribution of unproductive H_2O_2 decomposition in the case of **2**/H_2O_2/AA/**bna**, operating via the less reactive intermediate **2a**. The lower reactivity of **2a** compared to **1a** is in line with the higher **bna** epoxidation enantioselectivity of the system **2**/H_2O_2/AA, compared to the **1**/H_2O_2/AA system (59% *ee* vs. 35% *ee*, entry 7, Table 1 vs. entry 2, Table 1). Adding $HClO_4$ deteriorates the **bna** epoxidation enantioselectivity (from 59% to 51% *ee*) and reduces the epoxide yield (cf. entry 8 vs. 7, Table 1) at the same time. If one uses EHA instead of AA, the drop of the epoxide yield is more pronounced (from 58% to only 2%, cf. entry 10 vs. 9, Table 1). This negative effect is even more significant than in the system **1**/H_2O_2/EHA/($HClO_4$)/**bna** (cf. entries 4 and 5 of Table 1).

Overall, adding $HClO_4$ (2 equiv. vs. Fe) to the system **1**/H_2O_2/AA/**bna** has been shown to improve the epoxide yield and at the same time, the epoxidation enantioselectivity, whereas for the system **2**/H_2O_2/AA/**bna,** this trend is not the case.

2.3. Regioselective Oxidation of Adamantane by the Catalyst Systems 1/H_2O_2/AA and 2/H_2O_2/AA

The systems discussed in the previous section have been compared in the regioselective oxidation of adamantane (**ada**) (Table 2). Like with **bna** epoxidation, the system **1**/H_2O_2/AA/$HClO_4$ demonstrates higher conversion in **ada** oxidation than the systems **1**/H_2O_2/AA and **1**/H_2O_2/$HClO_4$ (72.1% vs. 59.2 and 17.5%, entry 3 vs. entries 2 and 1, Table 2). Noticeably, the adamantane oxidation regioselectivity (reflected by normalized 3°/2° ratio) is higher for the catalyst systems **1**/H_2O_2/AA and **1**/H_2O_2/AA/$HClO_4$ (40–42 vs. 18, entries 3 and 2 vs. entry 1, Table 2), which behavior is similar to the pro-

gressive **bna** epoxidation enantioselectivity enhancement when passing from the system **1**/H_2O_2/$HClO_4$ to **1**/H_2O_2/AA and further to **1**/H_2O_2/AA/$HClO_4$ (Table 1).

Table 2. The effect of $HClO_4$ on the regioselective oxidation of adamantane with H_2O_2 in the presence of complexes **1** and **2** [a].

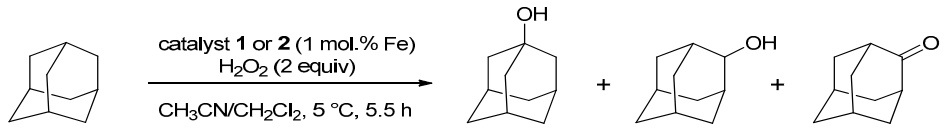

Entry	Catalyst	Carboxylic Acid	Strong Acid	Conversion (%)	1-ol:2-ol:2-one	3°/2° [b]
1	**1**	—	$HClO_4$	17.5	15.0:1.8:0.7	18.0
2 [c]	**1**	AA	—	59.2	55.1:1.7:2.4	40.0
3	**1**	AA	$HClO_4$	72.1	67.3:0.5:4.3	42.1
4	**2**	—	$HClO_4$	9.8	8.1:1.3:0.4	14.3
5 [c]	**2**	AA	—	48.4	43.3:4.0:1.1	25.4
6	**2**	AA	$HClO_4$	57.9	53.1:1.5:2.6	38.8

[a] At 5 °C, [catalyst]:[substrate]:[H_2O_2]:[acetic acid]]:[catalyst]:[$HClO_4$] = 0.5 μmol:100 μmol:200 μmol:110 μmol: 3 μmol; oxidant was added by a syringe pump over 30 min, and the mixture was stirred for an additional 5 h, followed by GC analysis. [b] 3°/2° = 3 × [1-adamantanol]/([2-adamantanol] + [2-adamantanone]). [c] From ref. [53].

The catalyst system **2**/H_2O_2/$HClO_4$ oxidizes adamantane with low conversion (9.8%, entry 4, Table 2), much lower than for the system **2**/H_2O_2/AA (48.4%, entry 5, Table 2). Like for the system **1**/H_2O_2/AA (cf. Table 2), adding $HClO_4$ to the **2**/H_2O_2/AA noticeably improves the conversion of adamantane oxidation (from 48.4% to 57.9%, entries 5 and 6, Table 2). The oxidation regioselectivity (3°/2° ratio) also increases when passing from the system **2**/H_2O_2/$HClO_4$ (3°/2° = 14.3) to the system **2**/H_2O_2/AA (3°/2° = 25.4) and further to **2**/H_2O_2/AA/$HClO_4$ (3°/2° = 38.8) (entries 4–6, Table 2).

In fact, the above data demonstrate that $HClO_4$ positively affects both the C-H oxidation regioselectivity and the product yield in the systems **1** or **2**/H_2O_2/AA/$HClO_4$/adamantane (Table 2), which holds considerable practical promise. Interestingly, this increase of regioselectivity is accompanied by the reactivity enhancement of the corresponding perferryl intermediates towards C-H oxidation (of cyclohexane, see Section 2.1). Even though it seems counterintuitive, this apparent violation of the "reactivity-selectivity" principle in C-H oxidation is not unusual for catalyst systems based on biomimetic catalysts of the Fe(PDP) family [50,51,53].

2.4. Chemo- and Regioselective Oxidation of (+)-Sclareolide by the Catalyst Systems 1/H_2O_2/AA and 2/H_2O_2/AA

Previously, (3a*R*)-(+)-sclareolide (**S**) was identified as, so far, the only substrate for which a uniform reactivity-selectivity correlation in C-H hydroxylations, mediated by iron-based catalysts of the Fe(PDP) family, has been documented [50,51]. The structures of the previously identified products of **S** oxidation are shown in Figure 5.

To probe the effect of $HClO_4$ on the chemo- and regioselectivity of the catalyst systems **1**/H_2O_2 and **1**/H_2O_2/AA in the oxidation of **S**, the following conditions were used: **1**/H_2O_2/$HClO_4$/**S** = 1:350:6:300; **1**/H_2O_2/AA/**S** = 1:350:250:300; and **1**/H_2O_2/AA/$HClO_4$/**S** = 1:350:250:6:300. The results are shown in Table 3. The addition of $HClO_4$ to the catalyst system **1**/H_2O_2/AA dramatically improves the conversion of **S** (from 20.6 to 50%, entries 2 and 3, Table 3), which is accompanied by an increase of C2 regioselectivity (from 50.9 to 56.5%, entries 2 and 3, Table 3). At the same time, the C2 hydroxylation *chemoselectivity* decreases (cf. $\mathbf{S_{2(eq)\text{-}OH}}/\mathbf{S_{2=O}}$ ratio drops from 1.57, entry 2, to 0.50, entry 3). Apparently, this drop is caused simply by a more pronounced ketonization of the C2 methylenic group at the much higher conversion. The catalyst system **1**/H_2O_2/$HClO_4$/**S** = 1:350:6:300 shows poor conversion, which observation is similar to that for the system **1**/H_2O_2/$HClO_4$/**ada** (cf. entry 1 of Table 2).

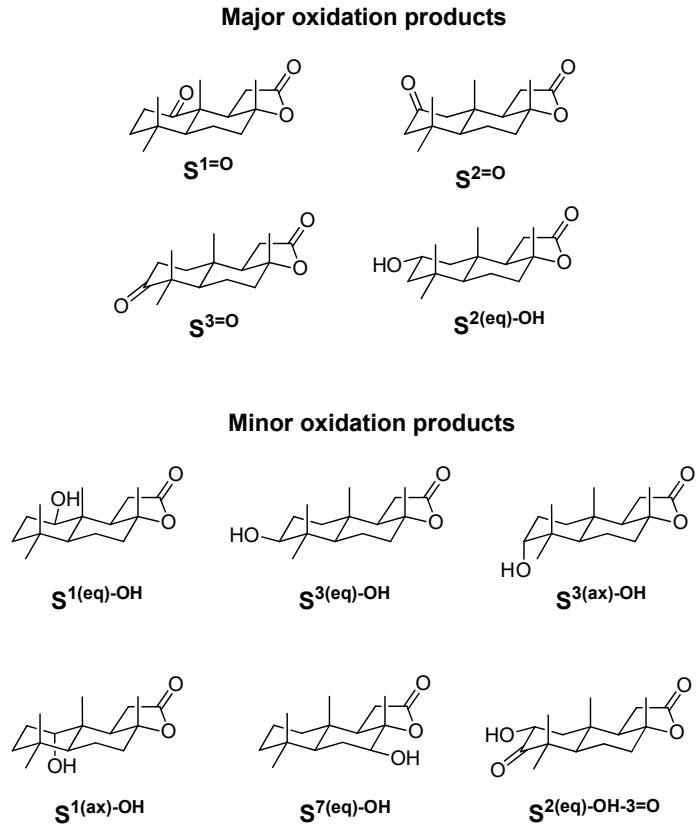

Figure 5. Structures of major and minor products of oxidation of (3a*R*)-(+)-sclareolide.

Table 3. The effect of $HClO_4$ on the product distribution of oxidation of (3a*R*)-(+)-sclareolide with H_2O_2 in the presence of complexes **1** and **2**.

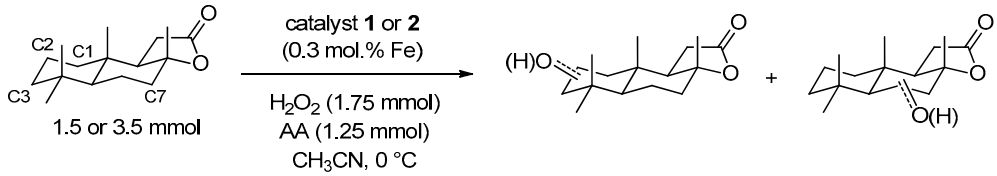

Entry	Cat.	Conv of S (%)	Products Distribution (%)										Regioseletivity (%)			
			$S^{3=O}$	$S^{2=O}$	$S^{1=O}$	$S^{2(eq)-OH}$	$S^{3(eq)-OH}$	$S^{3(ax)-OH}$	$S^{1(eq)-OH}$	$S^{1(ax)-OH}$	$S^{7(eq)-OH}$	$S^{2(eq)-OH-3=O}$	C1	C2	C3	C7
1 [a]	**1**	9.6	24.0	18.3	15.9	27.7	3.0	3.2	3.8	—	3.8	—	19.7	46.0	30.5	3.8
2 [b]	**1**	20.6	24.3	19.8	12.6	31.1	2.4	2.4	3.0	0.5	3.0	0.9	16.1	50.9	29.1	3.0
3 [c]	**1**	50	28.9	37.6	12.9	18.9	—	0.9	—	—	0.8	—	12.9	56.5	29.8	0.8
4 [d]	**2**	9.4	19.1	10.6	4.3	53.2	3.2	3.2	2.1	1.0	3.3	—	7.4	63.8	25.5	3.3
5 [e]	**2**	29	30.3	24.8	7.7	34.8	—	—	—	—	2.4	—	7.7	59.6	30.3	2.4

Reaction conditions: [a] **1**/H_2O_2/$HClO_4$/**S** = 1:350:6:300; [b] **1**/H_2O_2/AA/**S** = 1:350:250:300; [c] **1**/H_2O_2/AA/$HClO_4$/**S** = 1:350:250:6:300; [d] **2**/H_2O_2/AA/**S** = 1:350:250:300; [e] **2**/H_2O_2/AA/$HClO_4$/**S** = 2:350:250:6:300. Solvent CH_3CN; the oxidant was added by a syringe pump over 30 min at 0 °C, and the mixture was stirred for an additional 2.5 h at 0 °C, followed by a workup and a NMR analysis.

The catalyst system **2**/H_2O_2/AA/**S** = 1:350:250:300 demonstrates high regioselectivity towards the C2-methylenic site of **S** (63.8%, entry 4, Table 3). However, in contrast to the system **1**/H_2O_2/AA/**S** (see above), adding $HClO_4$ to the sample **2**/H_2O_2/AA/$HClO_4$/**S** = 1:350:250:6:300 results in a minor but noticeable drop of the C2 regioselectivity (59.6%, entry 5, vs. 63.8%, entry 4 of Table 3). At the same time, the C3 selectivity increases by ca. 5 percent points. In the case of **1**/H_2O_2/AA/**S** (see above), adding $HClO_4$ significantly improves the substrate conversion (29% vs. 9.4%, entries 5 and 4, Table 3).

3. Discussion

It is particularly interesting to rationalize the molecular mechanism of the simultaneous positive effect of $HClO_4$ on (1) the C-H oxidation reactivity, (2) product yield, and (3) oxidation regioselectivity of nonheme catalyst systems based on Fe complexes of the PDP family. Previously, it was established that Brønsted acids (such as HOTf and $HClO_4$) and Lewis acids (such as Sc^{3+}) are able to enhance the oxidizing power of nonheme Fe^{IV}=O complexes [36–44]. In some cases, this reactivity enhancement was discussed in terms of acid-triggered O-O bond heterolysis of a nonheme Fe^{III}(OOH) species, to facilitate formation of the active intermediates capable of hydroxylating strong C-H bonds [45,46]. However, in our case, this explanation is unsuitable, since the addition of $HClO_4$ to the intentionally generated key perferryl intermediates [(^{Me2OMe}PDP)Fe^{V}=O(OAc)]$^{2+}$ (**1a**) and [(^{NMe2}PDP)Fe^{V}=O(OAc)]$^{2+}$ (**2a**) has been shown to increase their self-decay rates and reactivity to cyclohexane (see Section 2.1).

Alternatively, it has been shown that strong acid (HOTf) can protonate the chelating ligand of the nonheme complex [(TAML)Fe^{V}=O]$^{-}$ at remote positions, thus increasing the electrophilicity of the nonheme iron(V) oxo complex and enhancing its reactivity in oxygen transfer (OT) and electron transfer (ET) reactions [56]. Strictly speaking, accepting such an explanation in our case would have left the question open, how the increased electrophilicity (and hence reactivity) fits together with increased oxidation regio- and enantioselectivity. Nevertheless, we have considered the hypothesis that $HClO_4$ protonates one of the remote NMe_2 groups of the active species [(^{NMe2}PDP)Fe^{V}=O(OAc)]$^{2+}$ (**2a**), and calculated the protonated state by DFT at the B3LYP/def2-TZVPP (for Fe)/6-311G(d) (for other atoms) level of theory (see Supporting Information for details).

One can see that NMe_2 mono-protonation is a moderately endergonic process (Figure 6), which in principle, might account for the enhanced electrophilicity of [(^{HNMe2}PDP)Fe^{V}=O(OAc)]$^{3+}$ (**2a^{NH+}**). However, the calculated Gibbs energies suggest that the equilibrium constant for its formation

$$K_{eq} = \frac{\left[\left(^{HNMe2}PDP\right)Fe^{V} = O(OAc)^{3+}\right]\left[ClO_4^{-}\right]}{\left[\left(^{HNMe2}PDP\right)Fe^{V} = O(OAc)^{2+}\right]\left[HClO_4\right]} \quad (1)$$

should not exceed 1×10^{-2} (at T = 273 K), which apparently rules out significant contribution of **2a^{NH+}** to the catalytic reaction. Furthermore, as mentioned above, this hypothesis does not bring additional understanding to the selectivity enhancement upon protonation.

On the other hand, one could consider protonation of the terminal oxygen atom of [(^{NMe2}PDP)Fe^{V}=O(OAc)]$^{2+}$ (**2a**) with $HClO_4$ to form [(^{NMe2}PDP)Fe^{IV}-OH(OAc)]$^{3+}$. Related models were invoked to explain the modulation of the catalytic properties of the ferryl complex[(N_4Py)Fe^{IV}(O)]$^{2+}$ by the additives of HOTf and $HClO_4$ [40,41]. Such protonation has been found to be exergonic (for both the S = 3/2 and S = 1/2) spin states (Figure 6), thus suggesting that adding $HClO_4$ should convert **2a** into predominantly [(^{NMe2}PDP)Fe^{IV}-OH(OAc)]$^{3+}$ (Supplementary Materials Figure S2). The latter species, owing to being protonated, may be expected to possess higher electrophilicity than the parent intermediate [(^{NMe2}PDP)Fe^{V}=O(OAc)]$^{2+}$ (**2a**), yet perhaps be incapable of breaking C-H bonds directly. We believe that [(^{NMe2}PDP)Fe^{IV}-OH(OAc)]$^{3+}$ (**2a^{OH+}**) could actually be considered as a reservoir of the active species. Being in fast dynamic equilibrium with the parent perferryl intermediate **2a**, the protonated reservoir species **2a^{OH+}** effectively "stabilizes" (in terms of decreasing free energy) the parent intermediate **2a**. This stabilization, in accordance with the Hammond−Leffler principle, should lead to more product-like transition states, thus resulting in higher oxidation selectivity.

In Supplementary Materials Figure S2, selected partial bond orders and spin densities for the intermediates ^{4}[(^{NMe2}PDP)Fe^{IV}-OH(OAc)]$^{3+}$ (^{4}**2a^{OH+}**) and ^{2}[(^{NMe2}PDP)Fe^{IV}-OH(OAc)]$^{3+}$ (^{2}**2a^{OH+}**) are presented and compared with those of the parent intermediate [(^{NMe2}PDP)Fe^{V}=O(OAc)]$^{2+}$ (**2a**) [50]. The electronic structures of the protonated-at-terminal

oxygen intermediates ^{4}**2a**$^{OH+}$ are best described as iron(IV)-hydroxo complexes, with the $S = 1$ at the Fe^{IV} center, coupled with the $S = 1/2$ located at the ligand, ferromagnetically in the case of ^{4}**2a**$^{OH+}$ or antiferromagnetically in the case of ^{2}**2a**$^{OH+}$.

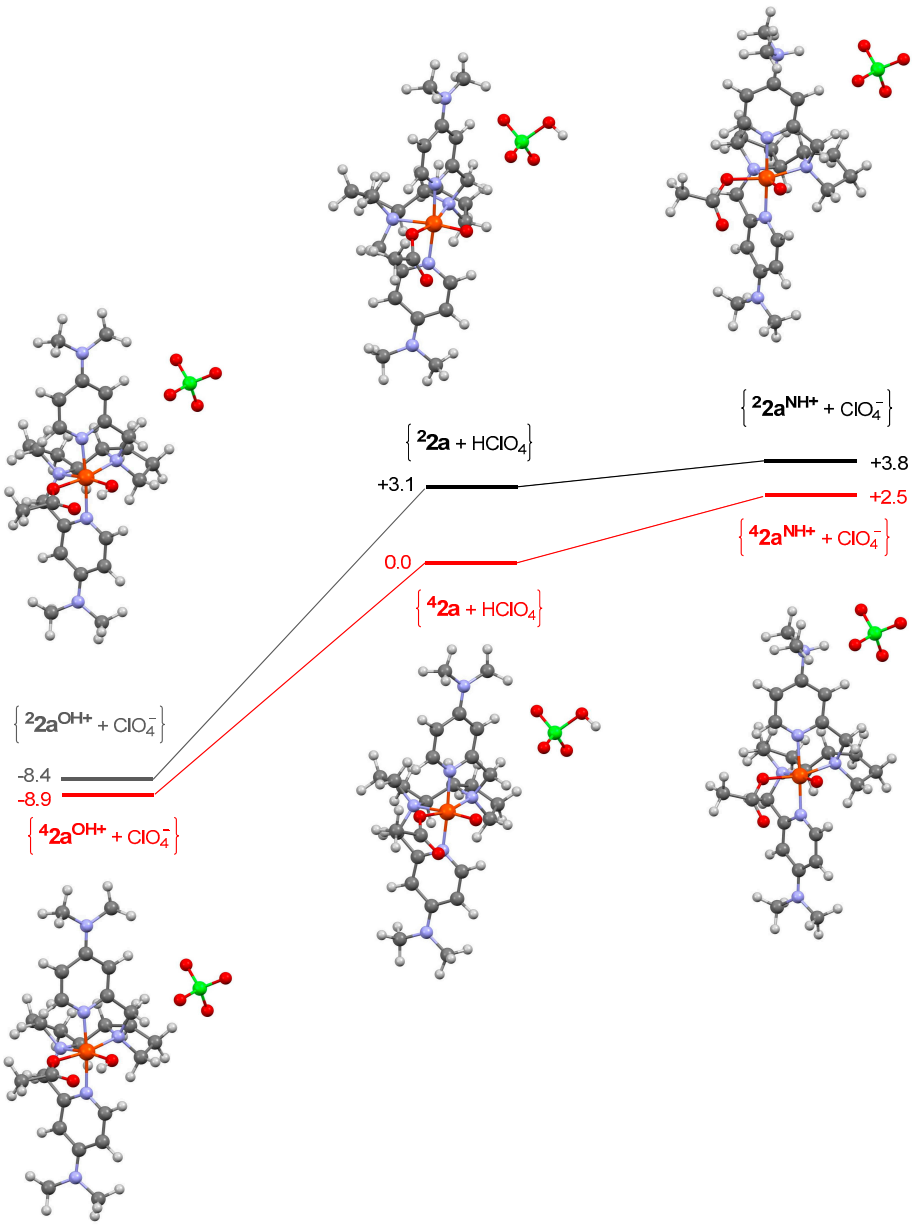

Figure 6. Optimized geometries and relative free energies (kcal/mol) of the non-protonated intermediates of the type {**2a** + $HClO_4$}, as well as protonated at ligand ({**2a**$^{NH+}$ + ClO_4^-}) and at terminal oxygen ({**2a**$^{OH+}$ + ClO_4^-} on the $S = 3/2$ (red) and the $S = 1/2$ (black) energy surfaces. C, grey; H, light grey; N, violet; O, red; Cl, green; Fe, orange.

Previously, it was reported that the protonation of the $[(N_4Py)Fe^{IV}(O)]^{2+}$ complex, with $HClO_4$ at the terminal Fe=O, eliminates the primary KIE for C-H bond breaking (mesitylene/d_{12}-mesitylene: k_H/k_D drops from 31 to 1.0), which was interpreted as a changeover of the mechanism from direct hydrogen atom transfer (HAT) to proton-coupled electron transfer (PCET) [40]. We have compared competitive oxidations of cyclohexane/d_{12}-cyclohexane in the absence and in the presence of $HClO_4$ and witnessed similar KIE values in all cases, which is characteristic of metal-mediated, rate-limiting C-H bond breaking (Supplementary Materials Table S1). This result indicates that in the case of

the intermediates **1a** and **2a**, adding $HClO_4$ does not lead to a mechanism changeover, thus additionally corroborating our proposal of the role of their protonated forms, **1a**$^{OH+}$ and **2a**$^{OH+}$, as reservoirs of the true active species.

4. Materials and Methods

4.1. Materials

All chemicals and solvents were purchased from Aldrich, Acros Organics or Alfa Aesar and were used without additional purification. Iron complexes $[(^{Me2OMe}PDP)_2Fe^{III}{}_2(\mu\text{-}OH)_2](OTf)_4$ (**1**) [47] and $[(^{NMe2}PDP)_2Fe^{III}{}_2(\mu\text{-}OH)_2](OTf)_4$ (**2**) [52] were prepared as described.

4.2. Instrumentation

EPR spectra (−196 °C) were measured in 3 mm quartz tubes on a CMS 8400 EPR spectrometer at 9.4–9.5 GHz, a modulation frequency of 100 kHz, and a modulation amplitude of 5 G. Experiments were conducted in a quartz finger Dewar filled with liquid nitrogen. EPR signals were quantified by double integration, with a frozen solution of chromium(III) acetylacetonate as a standard at −196 °C.

NMR spectra were measured on a Bruker Avance 400 NMR spectrometer at 400.13 MHz (^{1}H) and 100.61 MHz (^{13}C) in 5 mm and 10 mm cylindrical glass tubes at room temperature, using $CDCl_3$ as the solvent.

The epoxide yield and enantiomeric excess values were measured on a Bruker Avance 400 NMR spectrometer and Shimadzu LC-20 chromatograph (with Chiralcel OB-H chiral stationary phase), respectively, as previously reported [57]. Experimental uncertainty of *ee* measurements did not exceed ± 1%. The yields of adamantane oxidation products were determined using a DB-WAX capillary column [30 m × 0.25 mm × 0.25µm, He carrier gas] on an Agilent 6890N gas chromatograph with a flame-ionization detector, with an uncertainty of 2% [58].

4.3. Sample Preparation for EPR Measurements

Using a gas-tight microsyringe connected with a polyethylene capillary, an appropriate amount of H_2O_2 in 0.05 mL of a 1.8:1 CH_2Cl_2/CH_3CN mixture was added to the solution (0.15 mL) of the ferric complex and acetic acid at −70 °C directly in a quartz EPR tube (d = 3 mm). After stirring for 3 min with a polyethylene capillary at the required temperature, the sample was frozen by immersion in liquid nitrogen, and the EPR spectrum was measured at −196 °C.

4.4. General Catalytic Oxidation Procedure

The organic substrate and carboxylic acid were added to the solution of the iron complex in CH_3CN (0.4 mL), and the mixture was thermostated at 0 °C. Then, a calculated amount of 30% H_2O_2 was injected by a syringe pump over 30 min upon stirring at 0 °C. The resulting mixture was stirred for 2.5–5h at 0–5 °C (see Tables 1–3 for details). Iron was removed by short-column purification (eluent: acetone). Volatiles were evaporated, and the reaction mixtures were analyzed by NMR and HPLC (for Table 1, refs. [54,57] for details), GC (for Table 2, ref. [53] for details), or NMR (for Table 3, ref. [51] for details). In the absence of either the catalyst or H_2O_2, the oxidations did not occur.

5. Conclusions

The effect of strong Brønsted ($HClO_4$) acid on the reactivity and selectivity of the catalyst systems **1** and **2**/H_2O_2/AcOH, based on nonheme iron complexes of the PDP family, $[(^{Me2OMe}PDP)Fe^{III}(\mu\text{-}OH)_2Fe^{III}(^{MeOMe2}PDP)](OTf)_4$ (**1**) and $[(^{NMe2}PDP)Fe^{III}(\mu\text{-}OH)_2Fe^{III}(^{NMe2}PDP)](OTf)_4$ (**2**), toward benzylideneacetone (**bna**), adamantane (**ada**), and (3a*R*)-(+)-sclareolide (**S**) has been examined. Adding $HClO_4$ to the catalyst systems **1** and **2**/H_2O_2/AcOH results in an enhancement of the catalytic efficiencies (turnover numbers or product yields) of these systems in C-H oxidation reactions and at the same time, increases the oxidation regioselectivity.

For the system **1**/H_2O_2/AcOH, a similar, simultaneous increase of catalytic efficiency and (enantio)selectivity upon addition of $HClO_4$ has been documented in the asymmetric epoxidation of **bna**. EPR spectroscopic monitoring has witnessed a threefold increase of reactivity (second-order rate constant) of the intermediate $[(^{Me2OMe}PDP)Fe^{V}{=}O(OAc)]^{2+}$ (**1a**) towards cyclohexane at −70 °C upon the addition of $HClO_4$. At the same time, the spectral parameters of **1a** did not noticeably change, thus witnessing that $HClO_4$ does not affect the first coordination sphere of the central atom. DFT modeling corroborates the hypothesis that the positive effect of strong acid could be due to the protonation of the terminal Fe=O moiety of the parent perferryl intermediates to form species of the type $[(L)Fe^{IV}\text{-}OH(OAc)]^{3+}$, which should be more electron-deficient than the parent perferryl species $[(L)Fe^{V}{=}O(OAc)]^{2+}$, yet may be not capable of breaking strong aliphatic C-H bonds directly. Instead, they could play the role of the reservoir of the active species, thus effectively stabilizing the active perferryl intermediates. This stabilization would lead to more product-like transition states, thus ensuring higher oxidation selectivity, whereas the increased electrophilicity of $[(L)Fe^{IV}\text{-}OH(OAc)]^{3+}$ leads to a higher apparent reactivity toward $C(sp^3)$-H groups of aliphatic substrates.

We believe that the above approach to the improvement of the catalytic reactivity of catalyst systems, based on the complexes of the PDP family, holds considerable promise for the future, and the proposed model of the effect of $HClO_4$ would contribute to disclosing the molecular mechanisms of the action of strong Brønsted acids on the catalytic reactivity of nonheme systems, thus extending the existing mechanistic landscape. Related studies, focused on establishing the peculiarities of the effect of Lewis acids on similar iron-based catalyst systems, are underway in our laboratory.

Supplementary Materials: The following supporting information can be downloaded at: https://www.mdpi.com/article/10.3390/catal12090949/s1, computational details, Cartesian coordinates and computed energies of the intermediates, Figure S1: Optimized geometries and relative free energies (kcal/mol) of the non-protonated intermediates of the type {2a+HOAc} as well as protonated at terminal oxygen $\{2a^{NH+}{+}AcO^{-}\}$-on the S = 3/2 (red) and the S = 1/2 (black) energy surfaces. C grey, H light grey, N violet, O red, Cl green, Fe orange; Figure S2: Selected computed partial bond orders and spin densities, and formal structural representations for the densities (in numbers of spins) for the intermediates $^{4}[(^{NMe2}PDP)Fe^{IV}\text{-}OH(OAc)]^{3+}$ ($^{4}2a^{OH+}$) and $^{2}[(^{NMe2}PDP)Fe^{IV}\text{-}OH(OAc)]^{3+}$ ($^{2}2a^{OH+}$), compared with those for the parent intermediate $[(^{NMe2}PDP)Fe^{V}{=}O(OAc)]^{2+}$ (2a). Bond orders and spin densities and are in black and red, respectively; Table S1: Kinetic isotope effects for the oxidations of cyclohexane/d12-cyclohexane on catalysts 1 and 2 in the absence and in presence of $HClO_4$[a].

Author Contributions: Conceptualization, K.P.B. and E.P.T.; validation, A.M.Z. and D.E.B.; formal analysis, A.M.Z., A.A.B., D.E.B. and O.Y.L.; investigation, A.M.Z., A.A.B. and D.E.B.; resources, E.P.T., K.P.B. and O.Y.L.; writing-original draft preparation, E.P.T. and K.P.B.; writing-review and editing, A.M.Z., K.P.B., E.P.T. and O.Y.L.; visualization, A.M.Z. and K.P.B.; supervision, E.P.T. and K.P.B.; project administration, E.P.T.; funding acquisition, E.P.T. All authors have read and agreed to the published version of the manuscript.

Funding: The authors thank the Russian Science Foundation (grant 22-13-00225) for their financial support.

Data Availability Statement: Not applicable.

Acknowledgments: AAB acknowledges the access to the supercomputer facilities of the Computing Centre of Novosibirsk State University. The access to the facilities of the shared research center at the National Center of Investigation of Catalysts," kindly provided by the Boreskov Institute of Catalysis, is also acknowledged.

Conflicts of Interest: The authors declare no conflict of interest.

References

1. Guengerich, F.P. Mechanisms of Cytochrome P450-Catalyzed Oxidations. *ACS Catal.* **2018**, *8*, 10964–10976. [CrossRef]
2. Huang, X.; Groves, J.T. Oxygen Activation and Radical Transformations in Heme Proteins and Metalloporphyrins. *Chem. Rev.* **2018**, *118*, 2491–2553. [CrossRef]
3. Guo, M.; Corona, T.; Ray, K.; Nam, W. Heme and Nonheme High-Valent Iron and Manganese Oxo Cores in Biological and Abiological Oxidation Reactions. *ACS Cent. Sci.* **2019**, *5*, 13–28. [CrossRef]
4. Larson, V.A.; Battistella, B.; Ray, K.; Lehnert, N.; Nam, W. Iron and Manganese Oxo Complexes, Oxo Wall and Beyond. *Nat. Rev. Chem.* **2020**, *4*, 404–419. [CrossRef]
5. Baglia, R.A.; Zaragoza, J.P.T.; Goldberg, D.P. Biomimetic Reactivity of Oxygen-Derived Manganese and Iron Porphyrinoid Complexes. *Chem. Rev.* **2017**, *117*, 13320–13352. [CrossRef]
6. Yokota, S.; Fujii, H. Critical Factors in Determining the Heterolytic versus Homolytic Bond Cleavage of Terminal Oxidants by Iron(III) Porphyrin Complexes. *J. Am. Chem. Soc.* **2018**, *140*, 5127–5137. [CrossRef]
7. Rittle, J.; Green, M.T. Cytochrome P450 Compound I: Capture, Characterization, and C-H Bond Activation Kinetics. *Science* **2010**, *330*, 933–937. [CrossRef]
8. Yosca, T.H.; Ledray, A.P.; Ngo, J.; Green, M.T. A New Look at the Role of Thiolate Ligation in Cytochrome P450. *J. Biol. Inorg. Chem.* **2017**, *22*, 209–220. [CrossRef]
9. Mittra, K.; Green, M.T. Reduction Potentials of P450 Compounds I and II: Insight into the Thermodynamics of C-H Bond Activation. *J. Am. Chem. Soc.* **2019**, *141*, 5504–5510. [CrossRef]
10. Sacramento, J.J.D.; Goldberg, D.P. Factors Affecting Hydrogen Atom Transfer Reactivity of Metal-Oxo Porphyrinoid Complexes. *Acc. Chem. Res.* **2018**, *51*, 2641–2652. [CrossRef]
11. Nam, W.; Lee, Y.-M.; Fukuzumi, S. Hydrogen Atom Transfer Reactions of Mononuclear Nonheme Metal-Oxygen Intermediates. *Acc. Chem. Res.* **2018**, *51*, 2014–2022. [CrossRef]
12. Kal, S.; Que, L. Dioxygen Activation by Nonheme Iron Enzymes with the 2-His-1-Carboxylate Facial Triad That Generate High-Valent Oxoiron Oxidants. *J. Biol. Inorg. Chem.* **2017**, *22*, 339–365. [CrossRef]
13. Engelmann, X.; Monte-Pérez, I.; Ray, K. Oxidation Reactions with Bioinspired Mononuclear Non-Heme Metal-Oxo Complexes. *Angew. Chem. Int. Ed.* **2016**, *55*, 7632–7649. [CrossRef]
14. Puri, M.; Que, L. Toward the Synthesis of More Reactive $S = 2$ Non-Heme Oxoiron(IV) Complexes. *Acc. Chem. Res.* **2015**, *48*, 2443–2452. [CrossRef]
15. Nam, W.; Lee, Y.-M.; Fukuzumi, S. Tuning Reactivity and Mechanism in Oxidation Reactions by Mononuclear Nonheme Iron(IV)-Oxo Complexes. *Acc. Chem. Res.* **2014**, *47*, 1146–1154. [CrossRef]
16. McDonald, A.R.; Que, L. High-Valent Nonheme Iron-Oxo Complexes: Synthesis, Structure, and Spectroscopy. *Coord. Chem. Rev.* **2013**, *257*, 414–428. [CrossRef]
17. Ray, K.; Pfaff, F.F.; Wang, B.; Nam, W. Status of Reactive Non-Heme Metal-Oxygen Intermediates in Chemical and Enzymatic Reactions. *J. Am. Chem. Soc.* **2014**, *136*, 13942–13958. [CrossRef]
18. Guo, M.; Lee, Y.-M.; Fukuzumi, S.; Nam, W. Biomimetic Metal-Oxidant Adducts as Active Oxidants in Oxidation Reactions. *Coord. Chem. Rev.* **2021**, *435*, 213807. [CrossRef]
19. Lee, J.L.; Ross, D.L.; Barman, S.K.; Ziller, J.W.; Borovik, A.S. C-H Bond Cleavage by Bioinspired Nonheme Metal Complexes. *Inorg. Chem.* **2021**, *60*, 13759–13783. [CrossRef]
20. Kal, S.; Xu, S.; Que, L. Bio-inspired Nonheme Iron Oxidation Catalysis: Involvement of Oxoiron(V) Oxidants in Cleaving Strong C-H Bonds. *Angew. Chem. Int. Ed.* **2020**, *59*, 7332–7349. [CrossRef]
21. Dantignana, V.; Company, A.; Costas, M. Oxoiron(V) Complexes of Relevance in Oxidation Catalysis of Organic Substrates. *Isr. J. Chem.* **2020**, *60*, 1004–1018. [CrossRef]
22. Devi, T.; Lee, Y.-M.; Nam, W.; Fukuzumi, S. Metal Ion-Coupled Electron-Transfer Reactions of Metal-Oxygen Complexes. *Coord. Chem. Rev.* **2020**, *410*, 213219. [CrossRef]
23. Liu, Y.; Lau, T.-C. Activation of Metal Oxo and Nitrido Complexes by Lewis Acids. *J. Am. Chem. Soc.* **2019**, *141*, 3755–3766. [CrossRef]
24. De Oliveira, F.T.; Chanda, A.; Banerjee, D.; Shan, X.; Mondal, S.; Que, L., Jr.; Bominaar, E.L.; Munck, E.; Collins, T.J. Chemical and Spectroscopic Evidence for an Fe^{V}-Oxo Complex. *Science* **2007**, *315*, 835–838. [CrossRef]
25. Lyakin, O.Y.; Bryliakov, K.P.; Britovsek, G.J.P.; Talsi, E.P. EPR Spectroscopic Trapping of the Active Species of Nonheme Iron-Catalyzed Oxidation. *J. Am. Chem. Soc.* **2009**, *131*, 10798–10799. [CrossRef]
26. Kundu, S.; Thompson, J.V.K.; Ryabov, A.D.; Collins, T.J. On the Reactivity of Mononuclear Iron(V)Oxo Complexes. *J. Am. Chem. Soc.* **2011**, *133*, 18546–18549. [CrossRef]
27. Ghosh, M.; Singh, K.K.; Panda, C.; Weitz, A.; Hendrich, M.P.; Collins, T.J.; Dhar, B.B.; Sen Gupta, S. Formation of a Room Temperature Stable Fe^{V}(O) Complex: Reactivity Toward Unactivated C-H Bonds. *J. Am. Chem. Soc.* **2014**, *136*, 9524–9527. [CrossRef]
28. Collins, T.J.; Ryabov, A.D. Targeting of High-Valent Iron-TAML Activators at Hydrocarbons and Beyond. *Chem. Rev.* **2017**, *117*, 9140–9162. [CrossRef]
29. Ghosh, M.; Pattanayak, S.; Dhar, B.B.; Singh, K.K.; Panda, C.; Sen Gupta, S. Selective C-H Bond Oxidation Catalyzed by the Fe-BTAML Complex: Mechanistic Implications. *Inorg. Chem.* **2017**, *56*, 10852–10860. [CrossRef]

30. Warner, G.R.; Somasundar, Y.; Jansen, K.C.; Kaaret, E.Z.; Weng, C.; Burton, A.E.; Mills, M.R.; Shen, L.Q.; Ryabov, A.D.; Pros, G.; et al. Bioinspired, Multidisciplinary, Iterative Catalyst Design Creates the Highest Performance Peroxidase Mimics and the Field of Sustainable Ultradilute Oxidation Catalysis (SUDOC). *ACS Catal.* **2019**, *9*, 7023–7037. [CrossRef]
31. Pattanayak, S.; Cantú Reinhard, F.G.; Rana, A.; Gupta, S.S.; de Visser, S.P. The Equatorial Ligand Effect on the Properties and Reactivity of Iron(V) Oxo Intermediates. *Chem. Eur. J.* **2019**, *25*, 8092–8104. [CrossRef] [PubMed]
32. Serrano-Plana, J.; Oloo, W.N.; Acosta-Rueda, L.; Meier, K.K.; Verdejo, B.; García-España, E.; Basallote, M.G.; Münck, E.; Que, L., Jr.; Company, A.; et al. Trapping a Highly Reactive Nonheme Iron Intermediate That Oxygenates Strong C-H Bonds with Stereoretention. *J. Am. Chem. Soc.* **2015**, *137*, 15833–15842. [CrossRef] [PubMed]
33. Fan, R.; Serrano-Plana, J.; Oloo, W.N.; Draksharapu, A.; Delgado-Pinar, E.; Company, A.; Martin-Diaconescu, V.; Borrell, M.; Lloret-Fillol, J.; García-España, E.; et al. Spectroscopic and DFT Characterization of a Highly Reactive Nonheme Fe^{V}-Oxo Intermediate. *J. Am. Chem. Soc.* **2018**, *140*, 3916–3928. [CrossRef] [PubMed]
34. Pattanayak, S.; Jasniewski, A.J.; Rana, A.; Draksharapu, A.; Singh, K.K.; Weitz, A.; Hendrich, M.; Que, L.; Dey, A.; Sen Gupta, S. Spectroscopic and Reactivity Comparisons of a Pair of BTAML Complexes with Fe^{V}=O and Fe^{IV}=O Units. *Inorg. Chem.* **2017**, *56*, 6352–6361. [CrossRef] [PubMed]
35. Dantignana, V.; Serrano-Plana, J.; Draksharapu, A.; Magallón, C.; Banerjee, S.; Fan, R.; Gamba, I.; Guo, Y.; Que, L.; Costas, M.; et al. Spectroscopic and Reactivity Comparisons between Nonheme Oxoiron(IV) and Oxoiron(V) Species Bearing the Same Ancillary Ligand. *J. Am. Chem. Soc.* **2019**, *141*, 15078–15091. [CrossRef]
36. Fukuzumi, S.; Morimoto, Y.; Kotani, H.; Naumov, P.; Lee, Y.-M.; Nam, W. Crystal Structure of a Metal Ion-Bound Oxoiron(IV) Complex and Implications for Biological Electron Transfer. *Nat. Chem.* **2010**, *2*, 756–759. [CrossRef]
37. Morimoto, Y.; Kotani, H.; Park, J.; Lee, Y.-M.; Nam, W.; Fukuzumi, S. Metal Ion-Coupled Electron Transfer of a Nonheme Oxoiron(IV) Complex: Remarkable Enhancement of Electron-Transfer Rates by Sc^{3+}. *J. Am. Chem. Soc.* **2011**, *133*, 403–405. [CrossRef]
38. Prakash, J.; Rohde, G.T.; Meier, K.K.; Jasniewski, A.J.; Van Heuvelen, K.M.; Münck, E.; Que, L. Spectroscopic Identification of an Fe^{III} Center, Not Fe^{IV}, in the Crystalline Sc–O–Fe Adduct Derived from $[Fe^{IV}(O)(TMC)]^{2+}$. *J. Am. Chem. Soc.* **2015**, *137*, 3478–3481. [CrossRef]
39. Fukuzumi, S.; Ohkubo, K.; Lee, Y.-M.; Nam, W. Lewis Acid Coupled Electron Transfer of Metal-Oxygen Intermediates. *Chem-Eur. J.* **2015**, *21*, 17548–17559. [CrossRef]
40. Park, J.; Lee, Y.-M.; Nam, W.; Fukuzumi, S. Brønsted Acid-Promoted C-H Bond Cleavage via Electron Transfer from Toluene Derivatives to a Protonated Nonheme Iron(IV)-Oxo Complex with No Kinetic Isotope Effect. *J. Am. Chem. Soc.* **2013**, *135*, 5052–5061. [CrossRef]
41. Park, J.; Lee, Y.-M.; Ohkubo, K.; Nam, W.; Fukuzumi, S. Efficient Epoxidation of Styrene Derivatives by a Nonheme Iron(IV)-Oxo Complex via Proton-Coupled Electron Transfer with Triflic Acid. *Inorg. Chem.* **2015**, *54*, 5806–5812. [CrossRef] [PubMed]
42. Park, J.; Morimoto, Y.; Lee, Y.-M.; Nam, W.; Fukuzumi, S. Metal Ion Effect on the Switch of Mechanism from Direct Oxygen Transfer to Metal Ion-Coupled Electron Transfer in the Sulfoxidation of Thioanisoles by a Non-Heme Iron(IV)-Oxo Complex. *J. Am. Chem. Soc.* **2011**, *133*, 5236–5239. [CrossRef] [PubMed]
43. Morimoto, Y.; Park, J.; Suenobu, T.; Lee, Y.-M.; Nam, W.; Fukuzumi, S. Mechanistic Borderline of One-Step Hydrogen Atom Transfer versus Stepwise Sc^{3+}-Coupled Electron Transfer from Benzyl Alcohol Derivatives to a Non-Heme Iron(IV)-Oxo Complex. *Inorg. Chem.* **2012**, *51*, 10025–10036. [CrossRef] [PubMed]
44. Park, J.; Morimoto, Y.; Lee, Y.-M.; Nam, W.; Fukuzumi, S. Unified View of Oxidative C-H Bond Cleavage and Sulfoxidation by a Nonheme Iron(IV)-Oxo Complex via Lewis Acid-Promoted Electron Transfer. *Inorg. Chem.* **2014**, *53*, 3618–3628. [CrossRef]
45. Kal, S.; Draksharapu, A.; Que, L. Sc^{3+} (or $HClO_4$) Activation of a Nonheme Fe^{III}-OOH Intermediate for the Rapid Hydroxylation of Cyclohexane and Benzene. *J. Am. Chem. Soc.* **2018**, *140*, 5798–5804. [CrossRef]
46. Serrano-Plana, J.; Acuña-Parés, F.; Dantignana, V.; Oloo, W.N.; Castillo, E.; Draksharapu, A.; Whiteoak, C.J.; Martin-Diaconescu, V.; Basallote, M.G.; Luis, J.M.; et al. Acid-Triggered O-O Bond Heterolysis of a Nonheme Fe^{III}(OOH) Species for the Stereospecific Hydroxylation of Strong C-H Bonds. *Chem-Eur. J.* **2018**, *24*, 5331–5340. [CrossRef]
47. Lyakin, O.Y.; Zima, A.M.; Samsonenko, D.G.; Bryliakov, K.P.; Talsi, E.P. EPR Spectroscopic Detection of the Elusive Fe^{V}=O Intermediates in Selective Catalytic Oxofunctionalizations of Hydrocarbons Mediated by Biomimetic Ferric Complexes. *ACS Catal.* **2015**, *5*, 2702–2707. [CrossRef]
48. Zima, A.M.; Lyakin, O.Y.; Bryliakov, K.P.; Talsi, E.P. Direct Reactivity Studies of Non-Heme Iron-Oxo Intermediates toward Alkane Oxidation. *Catal. Commun.* **2018**, *108*, 77–81. [CrossRef]
49. Burger, R.M.; Peisach, J.; Horwitz, S.B. Activated Bleomycin. A Transient Complex of Drug, Iron, and Oxygen That Degrades DNA. *J. Biol. Chem.* **1981**, *256*, 11636–11644. [CrossRef]
50. Zima, A.M.; Lyakin, O.Y.; Bryliakova, A.A.; Babushkin, D.E.; Bryliakov, K.P.; Talsi, E.P. Reactivity vs. Selectivity of Biomimetic Catalyst Systems of the Fe(PDP) Family through the Nature and Spin State of the Active Iron-Oxygen Species. *Chem. Rec.* **2022**, *22*. [CrossRef]
51. Zima, A.M.; Babushkin, D.E.; Lyakin, O.Y.; Bryliakov, K.P.; Talsi, E.P. High-Spin and Low-Spin State Perferryl Intermediates: Reactivity-Selectivity Correlation in Fe(PDP) Catalyzed Oxidation of (+)-Sclareolide. *ChemCatChem* **2022**, *14*, e202101430. [CrossRef]

52. Zima, A.M.; Lyakin, O.Y.; Bryliakov, K.P.; Talsi, E.P. High-Spin and Low-Spin Perferryl Intermediates in Fe(PDP)-Catalyzed Epoxidations. *ChemCatChem* **2019**, *11*, 5345–5352. [CrossRef]
53. Zima, A.M.; Lyakin, O.Y.; Bryliakov, K.P.; Talsi, E.P. Low-Spin and High-Spin Perferryl Intermediates in Non-Heme Iron Catalyzed Oxidations of Aliphatic C-H Groups. *Chem. Eur. J.* **2021**, *27*, 7781–7788. [CrossRef] [PubMed]
54. Zima, A.M.; Lyakin, O.Y.; Bushmin, D.S.; Soshnikov, I.E.; Bryliakov, K.P.; Talsi, E.P. Non-Heme Perferryl Intermediates: Effect of Spin State on the Epoxidation Enantioselectivity. *Mol. Catal.* **2021**, *502*, 111403. [CrossRef]
55. Zima, A.M.; Lyakin, O.Y.; Ottenbacher, R.V.; Bryliakov, K.P.; Talsi, E.P. Dramatic Effect of Carboxylic Acid on the Electronic Structure of the Active Species in Fe(PDP)-Catalyzed Asymmetric Epoxidation. *ACS Catal.* **2016**, *6*, 5399–5404. [CrossRef]
56. Xue, S.-S.; Li, X.-X.; Lee, Y.-M.; Seo, M.S.; Kim, Y.; Yanagisawa, S.; Kubo, M.; Jeon, Y.-K.; Kim, W.-S.; Sarangi, R.; et al. Enhanced Redox Reactivity of a Nonheme Iron(V)-Oxo Complex Binding Proton. *J. Am. Chem. Soc.* **2020**, *142*, 15305–15319. [CrossRef]
57. Ottenbacher, R.V.; Samsonenko, D.G.; Talsi, E.P.; Bryliakov, K.P. Highly Enantioselective Bioinspired Epoxidation of Electron-Deficient Olefins with H_2O_2 on Aminopyridine Mn Catalysts. *ACS Catal.* **2014**, *4*, 1599–1606. [CrossRef]
58. Zima, A.M.; Lyakin, O.Y.; Bryliakov, K.P.; Talsi, E.P. On the Nature of the Active Intermediates in Iron-Catalyzed Oxidation of Cycloalkanes with Hydrogen Peroxide and Peracids. *Mol. Catal.* **2018**, *455*, 6–13. [CrossRef]